AIMS Materials Science, 8(2): 261–270.
DOI: 10.3934/matersci.2021017
Received: 18 January 2021
Accepted: 30 March 2021
Published: 19 April 2021

http://www.aimspress.com/journal/Materials

Research article

Capacitance response of solar cells based on amorphous Titanium dioxide (A-TiO_2) semiconducting heterojunctions

Hmoud. Al-Dmour*

Department of Physics, Faculty of Science, Mutah University, Mutah, 61710, Jordan

* **Correspondence:** Email: hmoud79@mutah.edu.jo.

Abstract: In the present study, we studied the capacitance frequency response of amorphous titanium dioxide (A-TiO_2)/poly(3-hexylthiophene) (P3HT) solar cells. The capacitance was measured to provide information on interfacial layer between the two materials. At a low frequency, the capacitance increased because the frequency was lower than the relaxation time of the charge carriers, thus providing evidence of the formation of a depletion region at the P3HT/A-TiO_2 interface. The loss tangent was measured for applied voltage ranging from 0 to 1.5 V and the frequencies from 20 Hz and 1 MHz. Peaks in the loss tangent appeared as a function of the applied voltage due to changes in the transport and accumulation mechanisms of charge at the interface and the presence of oxygen molecules in the TiO_2. The resulting C-V curves were used to calculate dopant concentration and the barrier's potential, which was found to 10^{17} cm^{-3} and 0.6 V, respectively. This confirmed the presence of a depletion region placed in the P3HT region and the validated barrier's potential effect on the open circuit voltage value. It was also shown that the light J-V characteristics of the A-TiO_2/P3HT solar cells were independent of the ambient conditions because the conductivity of P3HT and the depletion region were not affected.

Keywords: interfacial layer; loss tangent; amorphous TiO_2; barrier potential; relaxation time

1. Introduction

The importance of the organic-inorganic interfaces in solar cells for their operation and potential range of applications has been demonstrated by investigating the microscopic processes occurring within these devices [1,2]. It has been reported that using two or more layers and modifying the morphology of the components of solar cells affect the formation of the space charge region, the

mobility of charge carriers, trapping and recombination processes, and the stability of the resulting device. Organic-inorganic solar cells typically consist of many semiconductor layers in order to achieve high power conversion efficiency. For example, Pei et al. [3] fabricated a TiO_2 array/(P3HT) hybrid solar cell device in which the p-type organic semiconductor P3HT acts as a light absorber and a hole-transport material while the TiO_2 nanorod array acts as an electron-transport material, with an organic triphenylamine-type sensitizer employed to tune the interfacial characteristics of TiO_2/(P3HT), thus improving the compatibility between the TiO_2 nanorods and the polymer contact junction. Other types of solar cell contain two electron-transport materials and hole-transport material. They are fabricated by spin-coating a solution composed of electron-donating and electron-accepting materials (P3HT:PCBM) on to a metal oxide layer [4**]**. The interface between the components of these devices plays an important role in producing more efficient solar cells with higher stability and the ability to function in inclement weather conditions (e.g., during heavy rain or snowstorms) [5,6].

The main parameters of solar cells, including the power conversion efficiency *(η)*, short circuit current density (J_{sc}), and open-circuit voltage (V_{oc}), depend on the interface and the dielectric materials employed in their fabrication [7]. There is a consensus that the interface controls the four processes that occur within cells to generate photo-charges: photon absorption, exciton generation, exciton migration, exciton dissociation, charge transport and charge collection at the electrodes [8]. In addition to the junctions that form between the contacts (metal electrodes) and semiconductors, these processes are strongly associated with the energy difference between the lowest unoccupied molecular orbital (LUMO) of the electron-accepting material and the highest occupied molecular orbital (HOMO) of the donor at the interface in the active layer. These process have been studied using admittance a spectroscopic (AC) measurements, a technique that has been widely used by many researchers to identify the microscopic processes occurring within electronic devices and that is especially sensitive to interfacial effects related to the formation of depletion regions and to carrier transport trapping, and recombination processes [9].

In this article, we report on the capacitance response of heterojunction solar cells based on P3HTcoated on an amorphous titanium dioxide (A-TiO_2) thin film. Their behaviour was studied and compared with that of solar cells consisting of P3HT deposited onto mesoporous nanocrystalline titanium dioxide (nc-TiO_2). The results provide evidence that the formation of the interface and depletion region responds to changes in the applied frequency and voltage.

2. Materials and methods

In this study, heterojunction solar cells were fabricated using a thin layer of A-TiO_2 and P3HT acting as an active layer. Spin-coating was employed to deposit the TiO_2 film onto a pre-cleaned the fluorine-doped conducting tin oxide (FTO) glass plate (sheet glass, 8 Ω/sq, Solaronix), bottom electrode. This film was then sintered using the steps reported in [10]. During the sintering process, the sample turned from a milky colour at sintering temperatures of 70–80 ^oC to brown due to the burning of TiO_2 at sintering temperatures of 220–380 ^oC, leading to electrical contact between the composition of TiO_2. The final film was transparent when the temperature reached 450 ^oC. Figure 1a–c presents these changes in the colour of the sample. A solution of P3HT in chloroform (15 $mg \cdot mL^{-1}$) was prepared at ~45 ^oC to more rapidly advance dissolution. A drop of this solution was placed on the surface of the A-TiO_2 and left for several seconds prior to spinning at 1000 rpm.

The top electrode was made of gold and deposited on the active layer using a vacuum evaporator.

Figure 1d shows the pixels (circular shape) of the solar cells used in this study. An Agilent E4980A precision LCR meter was used to study the current versus voltage and capacitance versus voltage under different conditions. A xenon lamp was used to illuminate the device. For I-V measurements, Keithley 237 Source Measure Unit was used.

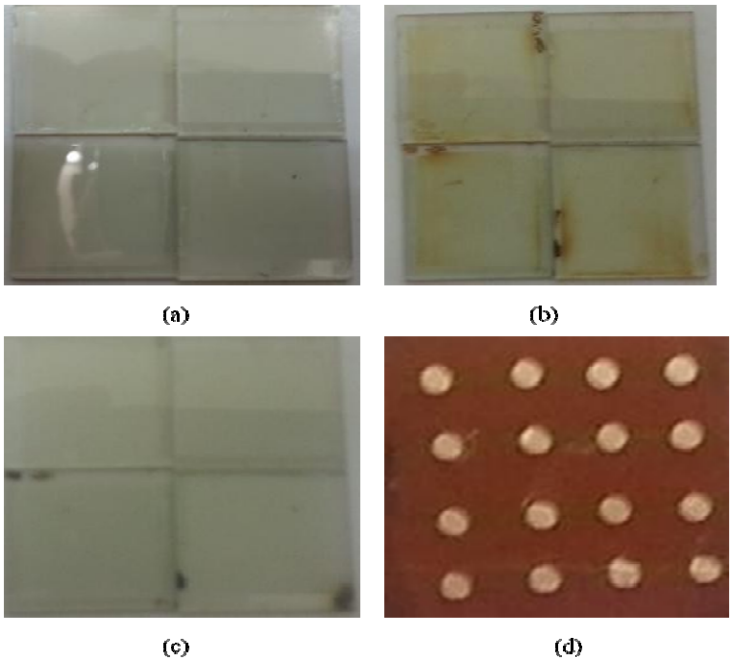

Figure 1. Images of the TiO_2 films sintered at (a) T = 70 ^oC, (b) T = 350 ^oC, (c) T = 450 ^oC, and (d) solar cell pixels.

3. Results and discussion

A low-angular-frequency signal voltage was applied to the SnO_2:Fn electrode. The charges concentration in the interfacial layer varied in response to the AC voltage across the solar cell. Complex dielectric permittivity measurements were used to identify the response of the solar cell to the electric field.

The apparent complex permittivity (ε^*) is given by Eq 1 [11]:

$$\varepsilon^* = \varepsilon' - i\varepsilon'' \tag{1}$$

where ε' is the real part of the permittivity, representing transport and charge storage through the bulk of the active layer, and ε'' is the imaginary part of the permittivity, representing the energy loss due to the movement of bound charges on the atoms and molecules in the changing electric current. According to a prior report [12], the device's capacitive and conductance effects are expressed using Eqs 2 and 3, respectively.

$$\varepsilon' = \frac{C}{C_g} = \varepsilon_\infty + \frac{\varepsilon_S - \varepsilon_\infty}{1+\omega^2\tau^2} \tag{2}$$

$$\varepsilon'' = \frac{G_m}{\omega C_g} = \frac{\omega\tau(\varepsilon_S - \varepsilon_\infty)}{1+\omega^2\tau^2} \tag{3}$$

where ε_s is the apparent value of the static permittivity (frequency = 0), ε_∞ (frequency = ∞) is the apparent value of the high-frequency permittivity, ω is the angular frequency, C is the measured capacitance, G_m is the conductance, and C_g is the geometric capacitance of the device calculated as follows in Eq 4 :

$$C_g = \frac{\varepsilon_o A}{d} \tag{4}$$

where A is the device area, and d is the sample thickness. The ratio of the imaginary part and the magnitude of the real part of the dielectric permittivity expressed in a complex form is the loss tangent, which is expressed as shown in Eq 5:

$$\tan\theta = \frac{\varepsilon''}{\varepsilon'} \tag{5}$$

Figure 2 shows the capacitance of the A-TiO_2/P3HTsolar cells over a wide range of measurement frequencies ($f = w/2\pi$) with different forward bias voltages applied to the bottom layer.

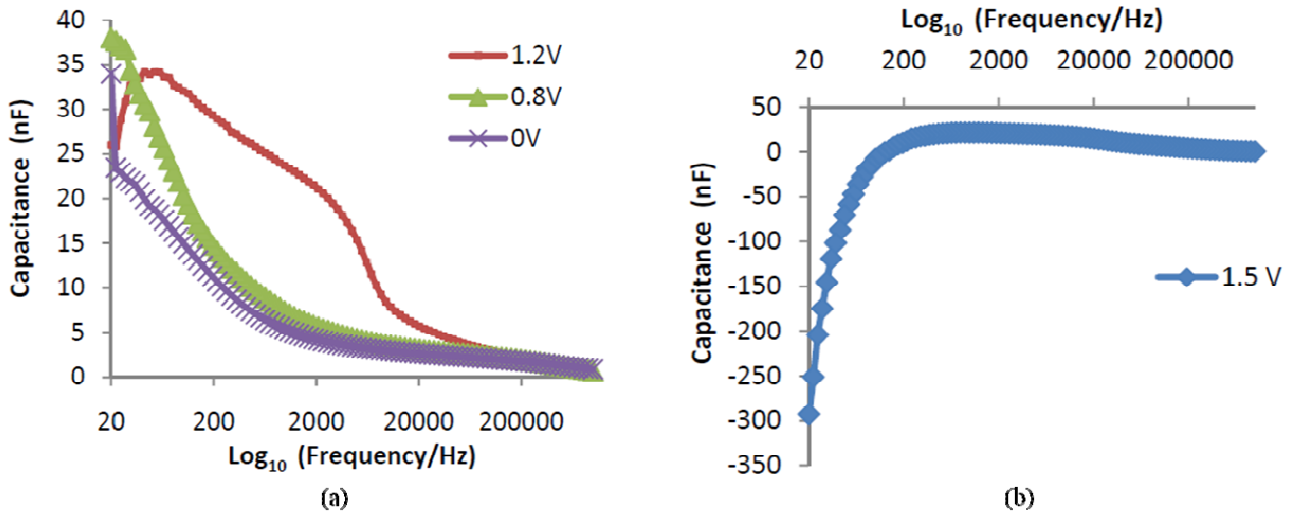

Figure 2. Frequency dependence of the capacitance of the A-TiO_2/P3HT solar cells measured in air at different voltage applied on SnO_2:F electrode (a) V = 0 V, 0.8 V and 1.2 V, (b) V = 1.5 V.

At the highest frequency (1 MHz), the capacitance was ~1 nF and this remained mostly constant as the applied voltage increased. This represents the geometric capacitance of the cell, and it occurs because the charge carriers cannot respond as quickly as the AC field varies over time, so the charge vibrations began to lag behind, reducing the capacitance. As demonstrated by Eq 4, there was an inverse relationship between the device thickness and its geometric capacitances. Thus, the thinner A-TiO_2 solar cell had a higher capacitance than the thicker solar cell in [13,14]. As the frequency decreased from 2000 to 20 Hz, the measured capacitance increased because the frequency was lower than the relaxation time of the charge carriers. This increase in the capacitance indicated the presence of an interfacial layer and depletion region at the P3HT/TiO_2 interface. The capacitance increased on the low-frequency side due to the effect of the forward bias voltage applied to the device. At 1.2 V, the capacitance increased to a maximum before decreasing from 35 to 25 nF. The capacitance was negative when the forward bias voltage was 1.5 V at 100 Hz. These results are explained by the equivalent circuit shown in Figure 3.

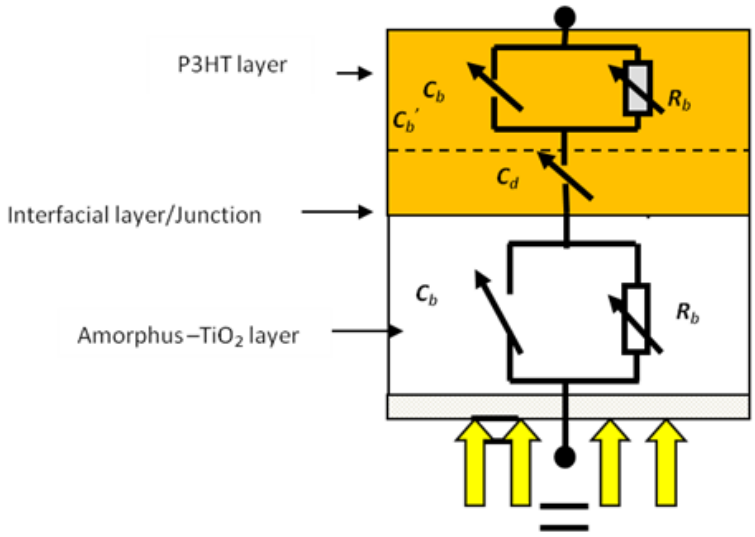

Figure 3. Equivalent circuit of an organic/inorganic solar cell.

The low-frequency capacitance was dominated by the interfacial layer or junction capacitance. It was associated with the static permittivity as shown in Eq 2. Under a forward bias, the charge carriers accumulated at the interface between the P3HT and A-TiO_2. As the charge carriers hopped from one site to another in the device and the components became polarised, the bulk region resistance (R_b) of the P3HTand A-TiO_2 decreased and weakened their bulk region capacitance (C_b). At a low frequency, an Increase in the C voltage from V = 0 V to 1.2 V reduced the barrier potential (V_{bi}) between the P3HT and A-TiO_2 and enhanced the accumulation of charge carriers. At 1.5 V, the junction capacitance (C_d) was dominated only by the diffusion capacitance, which increased the capacitance in the negative region of the C-f curve. This was produced by the injected charge carriers hopping from traps at the interface, but the time required for the charge carriers to hop at the interface was low, so the current lagged behind the applied voltage, becoming an inductive current or a negative capacitance [15]. Figure 4 presents the variation in the loss tangent dispersion factor (tan theta) of the P3HT/A-TiO_2 solar cells based on Eq 5 at different voltage biases. The device exhibited

a maximum loss tangent frequency of 2000 Hz when no forward bias was applied (see Figure 4a). As the frequency increased from 1000 to 10000 Hz, the tanδ values gradually decreased and became almost constant. At a DC forward voltage of 0.8 V, no maximum appeared at f = 2000 Hz, the same result as under zero bias (see Figure 4b). In addition, Figure 4c show sharp positive peak followed by a negative peak in the P3HT/A-TiO_2 solar cells was observed at a DC forward voltage of 1.5 V. Based on Stephen's report [16], the peaks observed in the loss tangent were attributed to the presence of moisture in the A-TiO_2. For the comparison with our previous work [13] on nanocrystalline TiO_2 (nc-TiO_2) solar cells, low tangent loss capacitance was observed in the A-TiO_2 device. The nc-TiO_2 became more conductive than A-TiO_2 because the morphology and porosity of nc-TiO_2 may have affected the polarization mechanisms that occurred when low signals voltage applied across the device. These results are in accordance with Wypych, who reported that [14]. The lowest loss tangent resulted from uniform grain structures and smaller grain boundary areas

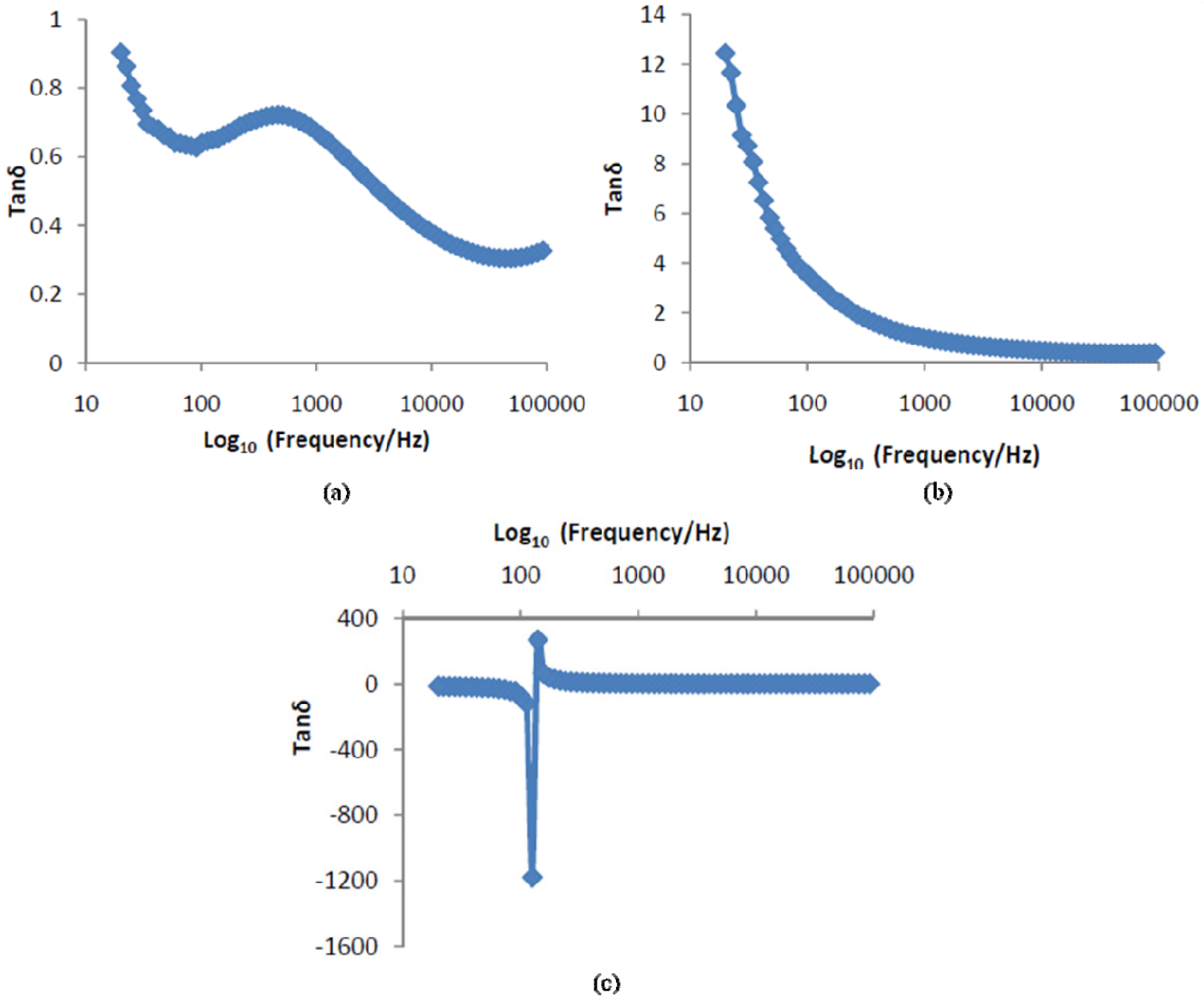

Figure 4. Frequency-dependence of the loss tangent corresponding to data in Figure 2. The measurements were mad with different applied bias voltages (a) V = 0 V, (b) V =0.8 V and (c) V = 1.5 V.

Due to their current density-voltage (J-V) characteristics, A-TiO_2/P3HT solar cells demonstrated high current rectification behaviour in dark conditions in [17]. By comparing the typical J-V curves of silicon p-n junction devices with J-V curve of A-TiO_2/P3HT solar cells, we assumed that a charge space region was created at the interface between P3HT and A-TiO_2. To illustrate this further, the capacitance-voltage characteristics of the A-TiO_2/P3HT solar cells when the voltage decreased from 1.5 V to −1.5 V are presented in Figure 5.

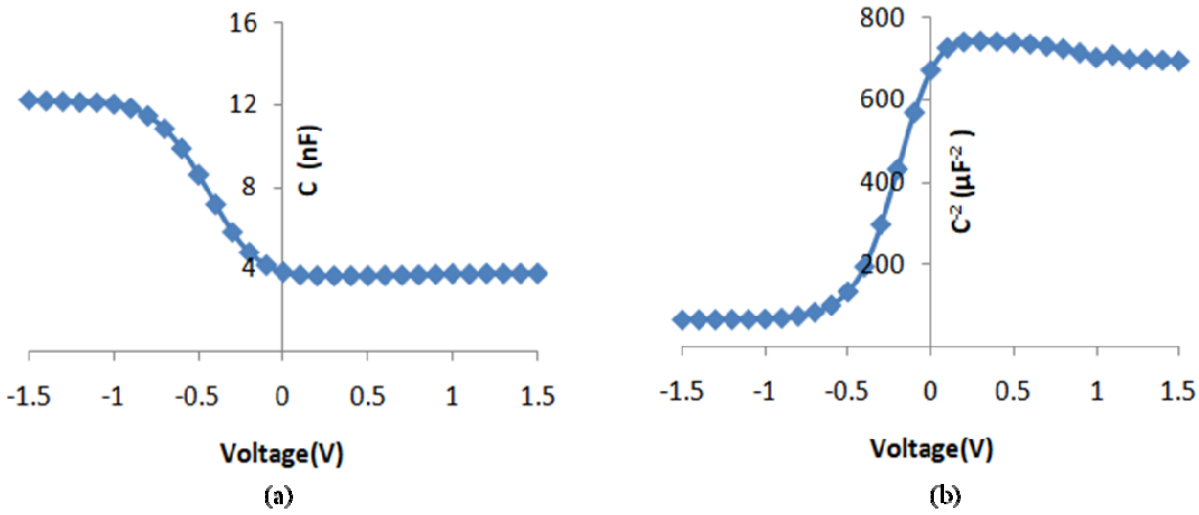

Figure 5. (a) Capacitance response of the A-TiO_2/P3HT solar cells at a 10 KHz in the dark, (b) C^{-2} vs V of the A-TiO_2/P3HT solar cells in the dark.

Figure 5a illustrates the increase and decrease in the width of the depletion region (depletion capacitance) or the accumulation of minority charges at the junctions (diffusion capacitance). However, because the C-V measurements were conducted at a high frequency, depletion capacitance dominated the measurements measurements. The capacitance sharply decreased when the voltage increased from −0.6 V to 0 V and reached a minimum of ~4 nF at −0.1 V, below which the capacitance was constant. This is in accordance with Eq 6, which shows that the depletion capacitance depends on the applied voltage [11]:

$$C^{-2} = \frac{2(V_{bi} - V)}{Aq\varepsilon\varepsilon_o N} \tag{6}$$

where N is the defect or acceptor doping density in the semiconductor component of the device, V is the applied potential, q is the electronic charge, A is the device area, ε_0 is the vacuum permittivity, ε is the relative dielectric constant of the components of solar cells and V_{bi} is the barrier potential. The barrier potential derives from the band bending of the two materials at the interface due to the difference in their Fermi energy levels. This was estimated by re-plotting the data in Figure 5b as C^{-2} versus V. The intercept of the extended linear portion of the C^{-2} and V plot with the voltage axis produced V_{bi} = 0.58, which is in agreement with the open-circuit voltage of the P3HT/A-TiO_2 solar cells (V_{oc} = 0.6) in [17] and was close to the difference between the Fermi energy levels of the two materials. The slope of the linear portion of C^{-2} and V plotted together with Eq 6 yielded an acceptor doping density (N_A) of 1.1 × 10^{17} cm^3 for the P3HT film. This is in good agreement with the doping

density of P3HT deduced by Torres [18] in their analysis of metal-insulator-semiconductor (MIS) structures incorporating P3HT. Conversely, the nc-TiO_2/P3HT solar cells had a low acceptor density and intercept for the extended linear portion of the C^{-2} and V plot with a voltage axis of V_{bi} = 1.21 V, which was close to its open-circuit voltage ($V_{oc} \approx 0.95$ V), and an acceptor charge density of 10^{14}. The results are shown in Figure 6a,b [17].

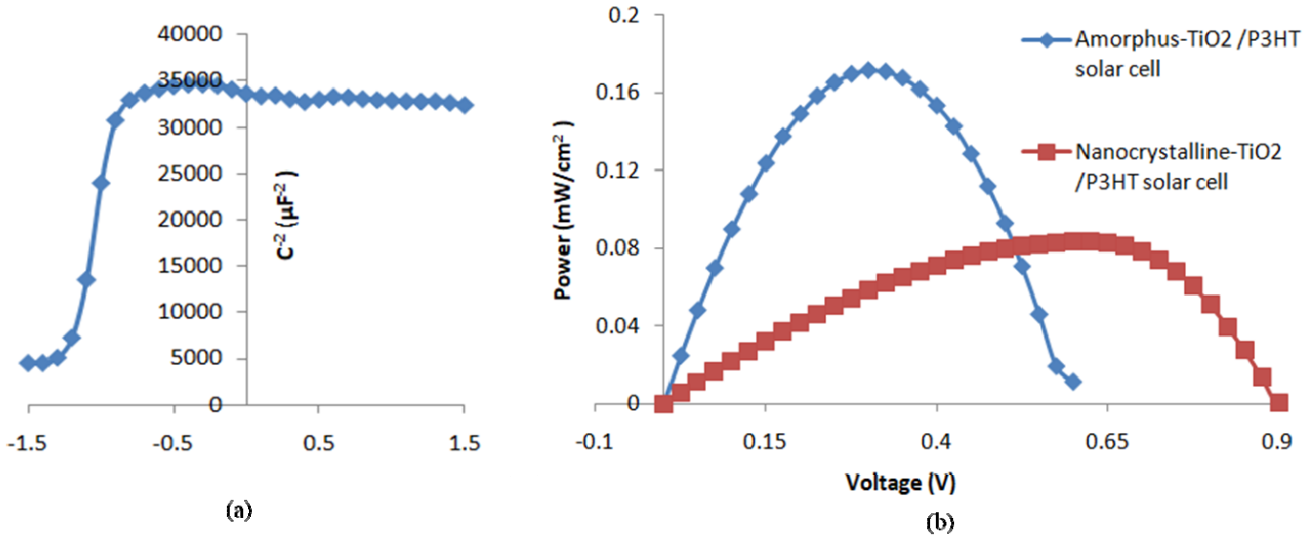

Figure 6. (a) C^{-2} vs V of the nc-TiO_2/P3HT solar cells in the dark. (b) Power vs voltage (P-V) characteristics of the nanocrystalline and amorphous TiO_2 solar cells [17].

These results confirmed that the A-TiO_2/P3HT solar cells had a depletion region on the P3HT side because the acceptor charge density was equal to the acceptor density obtained from the MIS solar cell. This explains the difference in the effect of ambient conditions on the A-TiO_2 solar cells when compared with nc-TiO_2 solar cells. In a previous study [18], the photovoltaic behaviour of nc-TiO_2/P3HT solar cells under illumination in a vacuum disappeared by reducing the doping concentration of P3HT, coupled with the electron-scavenging action of oxygen on the surface of thenc-TiO_2. This may have affected the formation of a depletion region on the two sides of the device, which is crucial for the open-circuit voltage and performance of metal oxide /organic solar cells. Figure 7 presents the current density-voltage characteristics of the A-TiO_2/P3HT solar cells in the dark and under illumination. Under a vacuum, the cell behaved as a solar cell, with V_{oc} = 0.5 V, J_{sc} = 0.01 mA/cm^2 and η = 0.01%. This suggests that ambient conditions have little influence on oxygen doping in P3HT, which produced a high dark current with a good rectification of approximately 10. Thus, the conductivity of A-TiO_2 was less sensitive to the vacuum, indicating that its pinhole- and nanoparticle- free surface reduced the electron-scavenging action of oxygen on the surface. The depletion region at the interface can thus be considered mainly responsible for the photovoltaic effect of a device composed of A-TiO_2 and P3HT layers.

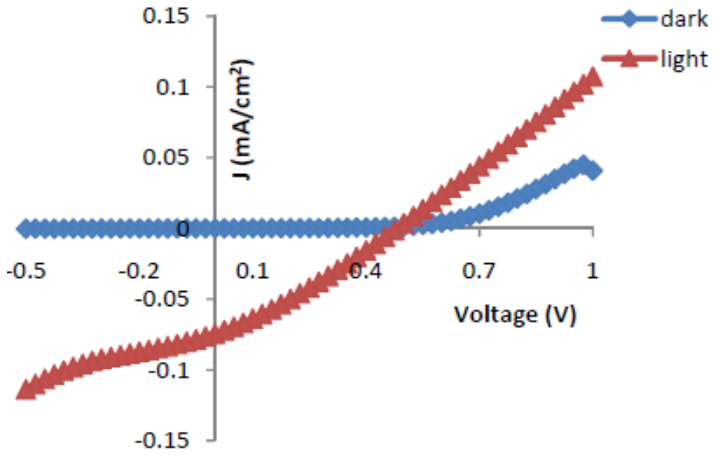

Figure 7. Current-voltage characteristics of an A-TiO_2/P3HT solar cell in a vacuum.

Under a high forward bias, the proposed device exhibited a higher current under illumination in comparison with the dark current under the same conditions, reaching around 0.15 mA/cm^2 at V = 1 V. This suggests that the conductivity of a material resulting from the absorption of optical photons is increased by the photoconductivity occurring in the bulk semiconductor region of the device [19].

4. Conclusion

We employed admittance spectroscopy measurements to study the interfacial layer between two different materials in a solar cell. The results showed that the capacitance depended on the frequency and voltage bias applied to the P3HT/A-TiO_2 solar cell, increasing as the frequency decreased and becoming negative at a high forward bias voltage of 1.5 V. We attributed this to the changes occurring in the charge accumulation at the interfacial layer and the width of the depletion region. Under zero bias, the tangent loss was low with one peak, and it disappeared when the applied voltage increased to 0.8 V and 1.5 V because, unlike nc-TiO_2 solar cells, there was an absence of pinholes and electron-scavenging oxygen on the A-TiO_2 surface. This was confirmed by the capacitance-voltage measurements, which were used to calculate an acceptor doping density of 10^{17} cm^{-3}. This was similar to the acceptor doping density of a P3HT MIS device in a vacuum and the air, while the barrier potential was found to be close to V_{oc} (0.6 V). This suggests that the depletion region was located in the P3HT region and this dominated the performance of the P3HT/A-TiO_2 solar cells. Thus, the effect of a vacuum on the performance of the A-TiO_2/P3HT solar cell was limited.

Conflict of interest

The authors declare that they have no conflict of interest.

References

1. Chikawa T, Shiratori S (2012) The influence of the organic/inorganic interface on the organic-Inorganic hybrid solar cells. *J Nanosci Nanotechnol* 12: 3725–3731.

2. Wan Z (2020) Interface passivation strategy improves the efficiency and stability of organic-inorganic hybrid metal halide perovskite solar cells. *J Mater Res* 35: 2166–2189.
3. Pei J, Hao YZ, Lv HJ, et al. (2016) Optimizing the performance of TiO_2/P3HT hybrid solar cell by effective interfacial modification. *Chem Phys Lett* 644: 127–131.
4. Yang P, Zhou X, Cao G, et al. (2010) P3HT:PCBM polymer solar cells with TiO_2 nanotube aggregates in the active layer. *J Mater Chem* 20: 2612–2616.
5. Raïssi M, Leroy-Lhez S, Ratier B (2016) Enhanced photocurrent and stability of organic solar cells using solution-based TS-CuPc interfacial layer. *Org Electron* 37: 183–189.
6. Dong X, Fang X, Lv M, et al. (2015) Improvement of the humidity stability of organic-inorganic perovskite solar cells using ultrathin Al_2O_3 layers prepared by atomic layer deposition. *J Mater Chem* 3: 5360–5367.
7. Cho A, Park N (2017) Impact of interfacial layers in perovskite solar cells. *ChemSusChem* 10: 3687–3704.
8. Jiang Y, Wang X, Pan A (2019) Properties of excitons and photogenerated charge carriers in metal halide perovskites. *Adv Mater* 31: 1806671.
9. Khelifi S, Decock K, Lauwaert J, et al. (2011) Investigation of defects by admittance spectroscopy measurements in poly (3-hexylthiophene):(6,6)-phenyl C61-butyric acid methyl ester organic solar cells degraded under air exposure. *Int J Appl Phys* 110: 094509.
10. Al-Dmour H, Taylor DM, Cambridge JA (2007) Effect of nanocrystalline-TiO_2 morphology on the performance of polymer heterojunction solar cells. *J phys D Appl Phys* 40: 5034–5038.
11. Sze M (1981) *Physics of Semiconductor Devices*, 2 Eds., New York: Wiley-Interscience.
12. Juarez-Perez EJ, Sanchez RS, Badia L, et al. (2014) Photoinduced giant dielectric constant in lead halide perovskite solar cells. *J Phys Chem Lett* 5: 2390–2394.
13. Al-Dmour H, Taylor DM (2011) Small-signal response of nanocrystalline-titanium dioxide/poly(3-hexylthiophene) heterojunction solar cells. *Thin Solid Films* 519: 8135–8138.
14. Wypych A, Bobowska I, Tracz M, et al. (2014) Dielectric properties and characterisation of titanium dioxide obtained by different chemistry methods. *J Nanomat* 2014: 124814.
15. Ghahremanirad E, Bou A, Olyaee S, et al. (2017) Inductive loop in the impedance response of perovskite solar cells explained by surface polarization model. *J Phys Chem Lett* 8: 1402–1406.
16. Stephen L (2020) Titanium dioxide versatile solid crystalline: An overview, In: Dongre RS, Peshwe DR, *Assorted Dimensional Reconfigurable Materials*, IntechOpen.
17. Al-Dmour H (2020) A comparative study of titanium dioxide preparation methods in solar cells based on the TiO_2 semiconducting polymer heterojunction. *IJAAS* 7: 133–138.
18. Torres I, Taylor DM (2005) Interface states in polymer metal-insulator-semiconductor devices. *Int J Appl Phys* 98: 073710.
19. Al-Dmour H, Taylor DM (2009) Revisiting the origin of open circuit voltage in nanocrystalline-TiO_2/polymer heterojunction solar cells. *Appl Phys Lett* 94: 223309.

AIMS Press